Pion Spectroscopy in Lattice QCD with $N_f = 2$ and Staggered Fermions

Institute for Theoretical Physics
Goethe Universität Frankfurt

Bachelorthesis

for gaining the academical grade
Bachelor of Science

presented by

Tim Breitenfelder
born 01/20/1994 in Bad Nauheim

in November 2016

1st supervisor:	Prof. Dr. Owe Philipsen
2nd supervisor:	JProf. Dr. Marc Wagner
advisor:	Ph.D. Alessandro Sciarra

Selbstständigkeitserklärung

Hiermit versichere ich, die vorliegende Abschlussarbeit meines Bachelorstudiums in Physik selbstständig und nur unter Verwendung der von mir angegebenen Quellen und Hilfsmittel verfasst zu haben. Sowohl inhaltlich als auch wörtlich entnommene Inhalte wurden als solche kenntlich gemacht. Die Arbeit hat in dieser oder vergleichbarer Form noch keinem anderem Prüfungsgremium vorgelegen.

Datum: _____ Unterschrift: _____

Zusammenfassung / Abstract

In this thesis the spectroscopy formalism in $N_f = 2$ lattice QCD with staggered fermions is studied and implemented into the CL^{2}QCD software for the case of pseudoscalar pions. The pion masses are measured for nonphysical bare quark masses in order to determine the structure of the QCD phase diagram.

In dieser Arbeit wird das Verfahren zur Spektroskopie in $N_f = 2$ Gitter-QCD mit staggered Fermionen hergeleitet und für die Messung von pseudoskalaren Pionen in die CL^{2}QCD Software implementiert. Die Pionenmassenbestimmung wird mit unphysikalischen Quark Massen vorgenommen und dient zur groben Bestimmung der Struktur des QCD Phasendiagramms.

Contents

List of Figures

1 Introduction

Today's well known matter consists all of 12 particles. There are 6 quarks, which are called up, down, strange, charm, bottom and top, and 6 leptons, namely the electron, muon and tau each with its neutrino partner. These particles interact in 4 different ways. There is the electromagnetic interaction and the weak interaction, which can be described together by the electroweak interaction, and the strong interaction, which is described by Quantum Chromodynamics (QCD).
Combined, these 12 particles and 3 interactions plus the higgs boson, which allows those particles to carry a mass, form up the Standard Model, the full description of particle physics. An overview of the Standard Model can be found in figure 1.1. The interactions in this theory are mediated by gauge bosons, which are the $W^{\pm}$ and Z^0 for all particles, the photon for all except the neutrinos and the gluons for the quarks only.

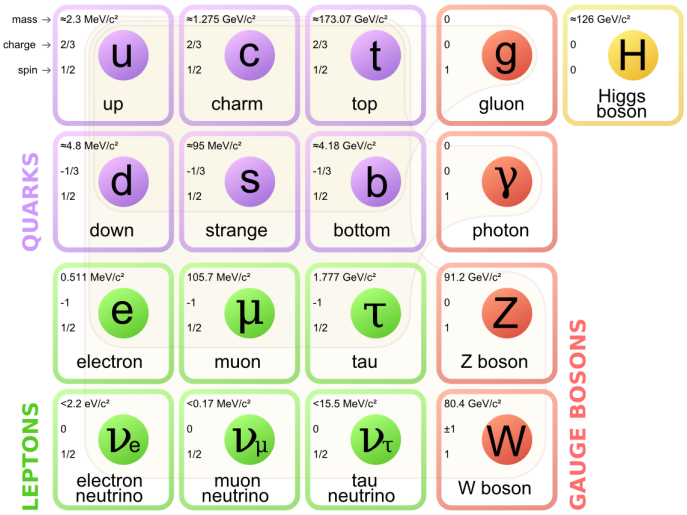

Figure 1.1: The Standard Model of particle physics, taken from ref. [1]

The 4th interaction, namely the gravitation, is described by Einstein's theory of General Relativity. Although both theories, the Standard Model and general relativity, theoretically contradict each other, the coexistence is legitimate because of the fact that the Standard Model only describes very short ranged interactions while general relativity has no measurable effect in those ranges.

Subject of current research is to find a great unified theory that is applicable for all four interactions.
Nevertheless, there are several hints, e.g. the probable existence of dark matter, outlining that there should be undiscovered particles in the universe that would disprove or enlarge the Standard Model. In this thesis we will focus on QCD only.

2 Theory

2.1 Continuum QCD

As already observed in the introduction sec. 1, Quantum Chromodynamics (QCD) is a quantum field theory for the description of the strong interaction. This interaction takes place between gluons and quarks, the constituents of protons and neutrons and therefore the elementary constituents of atomic nuclei.

In contrast to other gauge theories like Quantum Electrodynamics (QED), the quarks as interacting charged particles as well as the gluons as exchange particles carry color charge. These are three different colors and anti-colors, which are denoted by red, green and blue. Therefore, the underlying gauge group for QCD is the non-Abelian SU(3). Furthermore there are $3^2 - 1 = 8$ different gluons instead of for example only one uncharged photon in QED.

Due to gauge invariance, in nature one only observes colorless bound states as baryons and mesons. Whereas baryons consist of 3 quarks, each with a different color, so that the superposition of these colors is colorless, mesons contain two quarks, one with a certain color and the other with the corresponding anticolor. One meson particularly relevant for this thesis is the pion, which can have three different charges (π^+, its antiparticle π^- and π^0). For example, the mass of π^0 is known to be $134,9766(6)$ MeV [2]. With this mass, the pion is the lowest bound state in QCD and, therefore, the first state being excited, an important aspect in several studies.

In this thesis we will perform all calculations in euclidean spacetime which is obtained by performing a Wick rotation in Minkowski spacetime to the price of having to deal with complex time $\tau = i\,t$ instead of real t. Among others, one advantage is that euclidean spacetime is much more appropriate for numerical calculations.

Just like in any other theory, the basic element of QCD is its action, which can be divided in a fermionic part $S_F[\bar{\psi}, \psi, A]$ and a gluonic part $S_G[A]$. The

full euclidean continuum QCD action is given by (cf. [3, pp.27-31])

$$S[\bar{\psi}, \psi, A] = S_F[\bar{\psi}, \psi, A] + S_G[A] \tag{2.1}$$

$$S_F[\bar{\psi}, \psi, A] = \sum_{f=1}^{N_f} \int d^4x \; \bar{\psi}^{(f)}(x)[\gamma_\mu(\partial_\mu + iA_\mu(x)) + m^{(f)}]\psi^{(f)}(x) \tag{2.2}$$

$$S_G[A] = \frac{1}{2\,g^2} \int d^4x \; \mathrm{tr}[F_{\mu\nu}(x)F_{\mu\nu}(x)] \tag{2.3}$$

$$\text{with} \quad F_{\mu\nu}(x) = \partial_\mu A_\nu(x) - \partial_\nu A_\mu(x) + i[A_\mu(x), A_\nu(x)], \tag{2.4}$$

where $\psi(x)$ denotes the four component Dirac spinors representing fermionic fields, x is a euclidean spacetime four-vector, g is the coupling constant, $A_\mu(x)$ are the gluonic fields and γ_μ the Dirac matrices. Note that we used Einstein's sum convention and have no longer upper dirac indices in the euclidean case. The color degree of freedom is taken to be implicit in the equations above.
N_f specifies the total number of flavors entering the theory. Even though we already have seen that there are 6 different quark flavors in nature, we only take into account the two lightest ones, namely up and down ($N_f = 2$). This is a very useful assumption and can be justified with the argument that the masses of the other four quarks are much heavier and hence those states are rarely excited. Another helpful approximation is to assume degenerate masses for the up and down quarks,, i.e. set $m_u = m_d$, as the difference to the next higher quark mass m_s is about a factor of 40 respectively 20. Thus, in comparison of absolute values the up and down masses are quite small justifying this approximation although the down quark is as twice as heavy as the up quark. The handy thing about studying two-degenerate-flavor QCD is that chiral symmetry is preserved.

Because exact analytic calculations on measurable quantities fail in QCD and pertubative calculations only succeed in case of deconfinement at high energies ($g \to 0$), one needs to make use of different approaches for calculations. A very successful approach is lattice QCD (LQCD).

2.2 QCD on the Lattice

The aim of lattice QCD is to perform low energy QCD calculations numerically with the aid of computers. Thus it is mandatory to discretize the euclidean spacetime on a 4-dimensional lattice Λ with anti-periodic boundary conditions

$$\Lambda = \{n = (n_1, n_2, n_3, n_4) \,|\, n_1, n_2, n_3 = 0, 1, \ldots, N_S - 1;\; n_4 = 0, 1, \ldots, N_T - 1\} \quad . \tag{2.5}$$

The four dimensional vectors $n \in \Lambda$ label the spacetime points seperated by the lattice constant a which is the same for spatial and temporal directions.

The lattice unit vectors $\hat{\mu} \in \mathbb{Z}^4$ read

$$\hat{\mu} = (\delta_{1,\mu}, \delta_{2,\mu}, \delta_{3,\mu}, \delta_{4,\mu}) \quad . \tag{2.6}$$

We can take the continuum limit of quantities on the lattice by using the transformations

$$x \in \mathbb{R}^4 \to an,\ n \in \Lambda \tag{2.7}$$

$$\psi(x) \to \psi(an) \equiv \psi(n) \tag{2.8}$$

$$\partial_\mu \psi(x) \to \frac{1}{2a}[\psi(n+\hat{\mu}) - \psi(n-\hat{\mu})] \tag{2.9}$$

$$\int d^4x \to a^4 \sum_{n\in\Lambda} \quad . \tag{2.10}$$

With its finite volume and anti-periodic boundary conditions the lattice introduces a momentum cutoff and thus functions as a regulator for the QCD theory. The quantized momenta are restricted to the 1st Brillouin zone and in the continuum limit the momentum cutoff still remains. The path integral becomes mathematically well defined as it is transformed from a infinite dimensional integral to a finite dimensional integral. Furthermore the gauge field can be represented by a compact group, hence the path integral becomes finite without the need of gauge fixing. That is why the lattice provides a clean way to define a quantum field theory in general.
The problems of the lattice regularization are that Poincaré invariance as well as chiral symmetry for fermions are broken (staggered fermions are an exception). Besides, the finite volume introduces finite size effects and lattice artifacts such like fermion doublers (see next subsection) are introduced.

2.2.1 Naive Discretisation

Naively inserting the transformations (2.7) to (2.10) into the continuum fermionic action (2.5) leads to the naive discretized free fermion action $S_F^0[\psi, \bar{\psi}]$ ([3, p.33])

$$S_F^0[\psi, \bar{\psi}] = a^4 \sum_{n\in\Lambda} \bar{\psi}(n) \left[\sum_{\mu=1}^{4} \gamma_\mu \frac{\psi(n+\hat{\mu}) - \psi(n-\hat{\mu})}{2a} + m\psi(n) \right] \quad . \tag{2.11}$$

The propagator in momentum space reads

$$S_F^{0\,-1} = m + \frac{i}{a} \sum_{\mu=1}^{4} \gamma_\mu \sin(p_\mu a) \quad . \tag{2.12}$$

Due to the finite lattice spacing, the p_μ have to be inside the 1st Brioullin zone, which is usually taken to be the interval $[-\frac{\pi}{a}, \frac{\pi}{a}]$ for each dimension. Comparing the result from (2.12) with the continuum propagator, one notices

that the original momentum p_μ has been replaced by $\sin(p_\mu a) \equiv \tilde{p}_\mu$. For this reason, one obtains two additional roots per dimension which leads to 16 additional fermions instead of only one (see fig. 2.1).

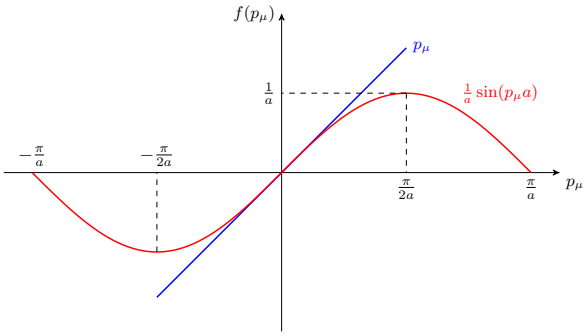

Figure 2.1: p_μ against $\tilde{p}_\mu \equiv \sin(p_\mu a)$. This figure shows the different behavior of the usual momentum p_μ and the *lattice momentum* $\tilde{p}_\mu$

These additional fermions are the so-called *doublers* and have no real physical analogue. In order to avoid the doublers, actions different from the naive one need to be chosen.
The first idea to face this problem was introduced by K. G. Wilson in the 70's. His idea was an explicit breaking of the chiral symmetry in order to give the doublers extremely high masses to decouple them from the theory in the continuum limit. An other approach to circumvent the doubling problem (besides Wilson fermions) are the so-called staggered fermions which are also known as Kogut-Susskind (KS) fermions.

2.2.2 Staggered Fermions

In the previous section, especially considering fig. 2.1, it is clear that the doubling problem with the naive fermion action occurs only at the edges of the Brillouin zone. The main idea of the staggered formulation (contrary to the Wilson approach, in which a counterterm is added to the mass) is to increase the lattice spacing and, thus, decrease the extent of the Brillouin zone.
The initial point for the derivation of the staggered action is again the naive discretized fermion action,

$$S = \frac{1}{2}\sum_{n,\mu}[\bar{\Psi}(n)\gamma_\mu(\Psi(n+\hat{\mu}) - \Psi(n-\hat{\mu}))] + M\sum_n \bar{\Psi}(n)\Psi(n) \quad . \tag{2.13}$$

In order to change the lattice spacing the action needs to be diagonal in Dirac space. Therefore unitary matrices $T(n) \in \mathbb{C}^{4\times 4}$ need to be found with the property [4, p.59]

$$T^\dagger(n)\,\gamma_\mu T(n \pm \hat{\mu}) = \eta_\mu\, \mathbb{1} \quad , \tag{2.14}$$

where the $\eta_\mu \in \mathbb{R}$ are the so-called *staggered phases*. The usual choice of $T(n)$ is

$$T(n) = \gamma_1^{n_1}\,\gamma_2^{n_2}\,\gamma_3^{n_3}\,\gamma_4^{n_4} \quad , \tag{2.15}$$

and the staggered phases are thus given by

$$\begin{cases} \eta_1 = 1 \\ \eta_\mu = (-1)^{\sum_{\nu<\mu} n_\nu} \end{cases} . \tag{2.16}$$

Transformation of the Spinors using $T(n)$ as defined in (2.15) yields to

$$\begin{cases} \Psi(n) \to T(n)\chi(n) \\ \bar{\Psi}(n) \to \bar{\chi}(n)T^\dagger(n) \end{cases} , \tag{2.17}$$

where we denote the so-called *staggered fields* with $\bar{\chi}(n)$,$\chi(n)$. At this point it is important to stress the fact that the staggered fields live on the finer lattice and do not have a direct physical meaning. Only the recombination of the staggered fields on the coarser lattice results in physical fields. Inserting (2.17) into (2.13) results in [4, p.59]

$$S = \frac{1}{2}\sum_{n,\mu}[\bar{\chi}(n)T^\dagger(n)\gamma_\mu T(n+\hat{\mu})\chi(n+\hat{\mu}) - \bar{\chi}(n)T^\dagger(n)\gamma_\mu T(n-\hat{\mu})\chi(n-\hat{\mu})] \tag{2.18}$$

$$+\hat{M}\sum_n \bar{\chi}(n)T^\dagger(n)T(n)\chi(n) \tag{2.19}$$

$$= \sum_{n,\mu,\alpha,\beta} \delta_{\alpha,\beta}\eta_\mu(n)\bar{\chi}_\alpha(n)\hat{\partial}^S_\mu\chi_\beta(n) + \hat{M}\sum_{n,\alpha,\beta}\delta_{\alpha,\beta}\bar{\chi}_\alpha(n)\chi_\beta(n) \tag{2.20}$$

It is easy to see that the action in the formulation above has indeed become diagonal in Dirac space, since the Dirac indices do only appear in the blue colored discrete Kronecker deltas. Therefore, one can now fix both Dirac indices, α and β, to a certain value. The most simple choice is certainly $\alpha = \beta = 1$. We obtain [4, p.59]

$$S_F^{(stag.)} = \frac{1}{2}\sum_{n,\mu}\eta_\mu(n)[\bar{\chi}(n)\chi(n+\hat{\mu}) - \bar{\chi}(n)\chi(n-\hat{\mu})] + M\sum_n \bar{\chi}(n)\chi(n) \tag{2.21}$$

The only remanent of the spin index are the staggered phases $\eta_\mu(n)$. It is important to pay attention to the fact that the staggered fields only have one component per lattice site. In continuum formulation, there are normally 4 spin indices, of course. Thus, (2.21) cannot be the final *physical* staggered action. One has to recombine the staggered fields, living on the original finer lattice, on a coarser lattice in order to be able to describe physics correctly. This is exactly the step where the basic idea of increasing the lattice spacing

enters.

This recombination of degrees of freedom takes the main part of staggering procedure and it is quite involved. We will not discuss it here in details and we will just focus on the result.
After some calculation, the action (2.21) can be written as ([4, sec. 4.5])

$$S_F^{(stag.)} = \sum_f \sum_N \bar{\Psi}^f(N)(\gamma_\mu \partial_\mu + M)\Psi^f(N) + \mathfrak{R} \quad , \tag{2.22}$$

where N labels the lattice sites of the coarser lattice. The term $\mathfrak{R}$ contains all the parts that vanish in the continuum limit. One can simply show that 2.22 indeed converges to the continuum QCD action in the limit of $a \to 0$. This is an important property for any fermion action and retrospectively legitimates the assumptions made to derive the staggered fermion action. Staggered fermions are preferred to Wilson fermions in situations where chiral properties dominate the system [5].

What also should be mentioned when talking about staggered fermions is the use of the *rooting trick* in the calculation of measurable quantities. Roughly speaking, a staggered lattice fermion corresponds to 4 continuum fermion tastes[1], therefore the determinant of the fermionmatrix for each quark flavor can be obtained by taking the 4th root of the corresponding staggered fermion matrix determinant (i.e. in Monte Carlo simulations). This rooting trick is mathematically questionable. Nevertheless using staggered fermions in LQCD has brought up results with unforeseen precision. A deeper insight into the rooting business is provided in ref. [6].

2.3 QCD Phase Diagram

The QCD phase diagram is of very high interest in recent theoretical physics research. In general, there are two phases that have been observed so far, namely the quark-gluon-plasma (QGP) and the usual hadronic matter. The quark-gluon-plasma is a state with a temperature of more than $\sim 175\, MeV$ (cf. [7]) at which the single quarks can be assumed as free particles due to the fact that the confinement is suspended. On the other hand the condensed (hadronic) matter resembles the present state in our everyday life at very low temperature. In this state the quarks combine and form up structures like protons and neutrons, which then may build atom cores etc. The important point is that in this phase the quarks obviously are subjected to a certain order unlike in the QGP case. Taking this into account, it is clear that there are

[1] The idea of taste does in general not coincide with the idea of flavor. For further details see ref. [4, sec 4.4]

2 different phases in which matter behaves differently. The major issue is to find out the type and the position of the phase transition between those two phases.

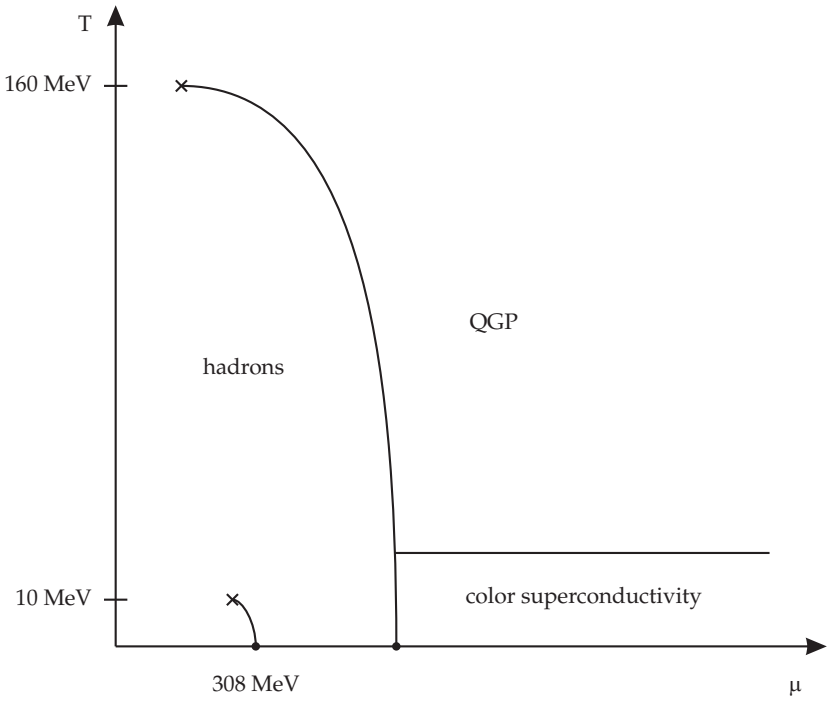

Figure 2.2: QCD phase diagram, taken from [8, p.3, figure 1]

Since those regions of very high energy in the QCD phase diagram are accessible via perturbation theory whereas regions of low energy are not, one has do apply different techniques.
In order to make qualitative statements on the type of the phase transition, it is helpful to have a look on the chiral symmetry of the $N_f = 2$ QCD action. Setting the quark masses $m_{u,d}$ to zero, the chiral symmetry of QCD is not explicitly but spontaneously broken, as indicated by the different masses of baryonic parity partners [3, pp. 161]. In contrast, in the QGP phase the chiral symmetry is not spontaneously broken. Since we have two phases with different symmetries, there must be a non analytic phase transition between hadronic matter and QGP.
If one switches over to the case of nonzero (but small) quark masses, the effect of the explicit symmetry breaking are not that tremendous, but then the chiral symmetry is spontaneously broken in both, the hadronic matter and the QGP phase. Therefore it should be possible to go from one to the other via a crossover. Actually, this crossover has been found using lattice calculations with staggered fermions [9, pp.21]. Moreover, increasing the baryonic density μ_B at zero temperature, one encounters a first order phase transition from the hadronic phase into the color superconducting phase, which we do

not want to discuss in this thesis. This first order phase transition was found by qualitative analysis based on effective chiral theories, because this regions are not reachable by lattice simulations, due to the sign problem (cf. [10, p. 21]). The presence of a crossover on the temperature axis and a first order phase transition on the baryonic density axis implies the existence of a critical point, at which the first order phase transition stops and becomes a crossover, comparable to the critical point of water[2].
The aim of the lattice calculations this thesis refers to is to study the order of the thermal transition of QCD at $\mu_B = 0$ varying the number and/or the mass of the quarks. Insights about the region at $\mu_B \neq 0$ with $\frac{\mu_B}{T} < 1$ can be obtained with several techniques.

2.3.1 Columbia Plot

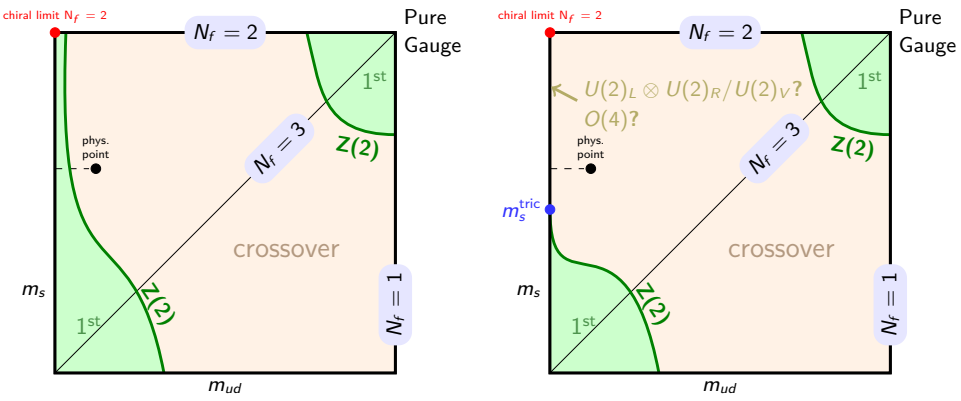

Figure 2.3: Two possible scenarios for structure of columbia plot at $\mu = 0$, taken from [11, p.2, figure 1]

A revealing and powerful instrument for the characterization of the QCD phase diagram is the Columbia plot. Analyzing the Columbia plot one is interested in the QCD phase transition for different degenerate up and down masses and different strange masses at a particular chemical potential μ_B [3]. Various regions in the Columbia plot differ in the order of phase transition one encounters when raising the temperature in the system.
A point of particular interest is, of course, the physical point, at which the quark masses take their physical bare values. In general, the behavior around the physical point allows conclusions concerning the physical point itself. Nevertheless, non-physical regions have interesting applications as well.

[2] Even though other possibilities could be realized, this is the simplest scenario.
[3] Historically the Columbia plot is only at $\mu_B = 0$. The extension to $\mu_B^2 < 0$ was done later on.

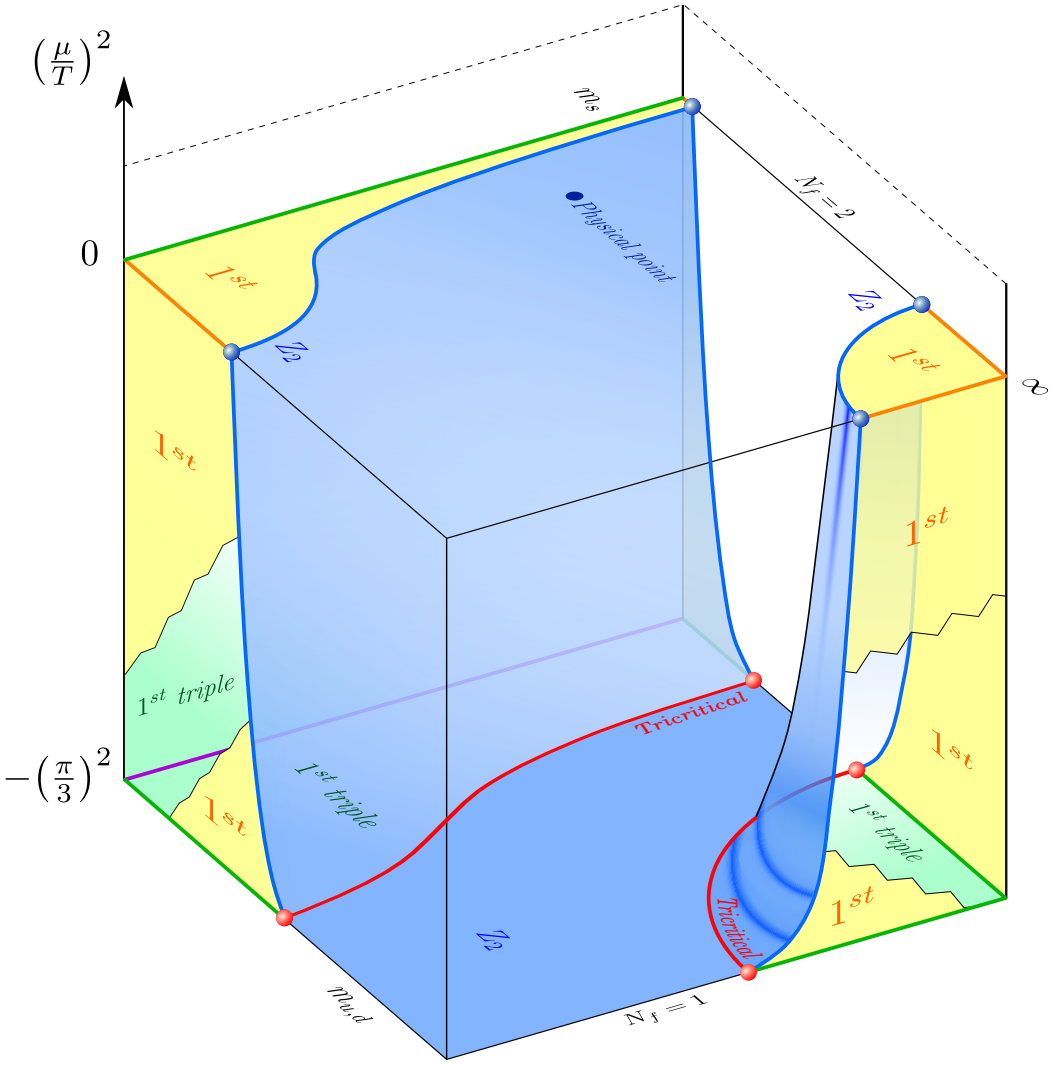

Figure 2.4: Columbia plot extended to imaginary chemical potential, taken from [14, p.2, figure 1]. The $N_f = 2$ plane is characterized by an infinite strange mass, i.e. $m_s \to \infty$, because having an infinite mass, the strange quark gets no longer excited and decouples from the theory. Thus, we only end up with up and down quarks and obtain an effective two flavor theory.

For example, for very small $m_{u,d}$, one can learn features about the chiral symmetry and for very high $m_{u,d}$, one enters the quenched state with quasistatic quarks. Figure 2.3 shows two possible scenarios for the historical Columbia plot at zero chemical potential.
As mentioned before, lattice QCD is unable to perform calculations for $\mu > 0$. Introducing a purely imaginary chemical potential, the sign problem disappears and lattice simulations become possible. This is why in the 3D columbia plot the third axis is specified with μ^2.

This imaginary chemical potential has a lower boundary at $(\frac{\mu}{T})^2 = -(\frac{\pi}{3})^2$, after which the partition function becomes periodic and therefore uninteresting from this point on [12]. This lower boundary is called Roberge-Weiss-plane.
One possible strategy to make predictions for real chemical potential is to extrapolate the results obtained at $\mu^2 < 0$ [13]. The Roberge-Weiss-plane is of great interest because it represents the starting point for these interpolations and lattice calculations are often cheaper. The following figure 2.4 sketches the structure of the Columbia plot with imaginary chemical potential including the Roberge-Weiss-plane.
This thesis is about calculating the pion mass m_π^{tric} at the heavier tricritical point on the $N_f = 2$ edge of the RW plane. In finite temperature LQCD the temperature is given by $T = \frac{1}{a \cdot N_\tau}$ and since the lattice spacing depends on the coupling of the theory, i.e. $a = a(\beta)$, T can be varied at fixed N_τ by changing β. This is a standard technique and the continuum limit can then be taken by repeating the same measurement for increasing N_τ.

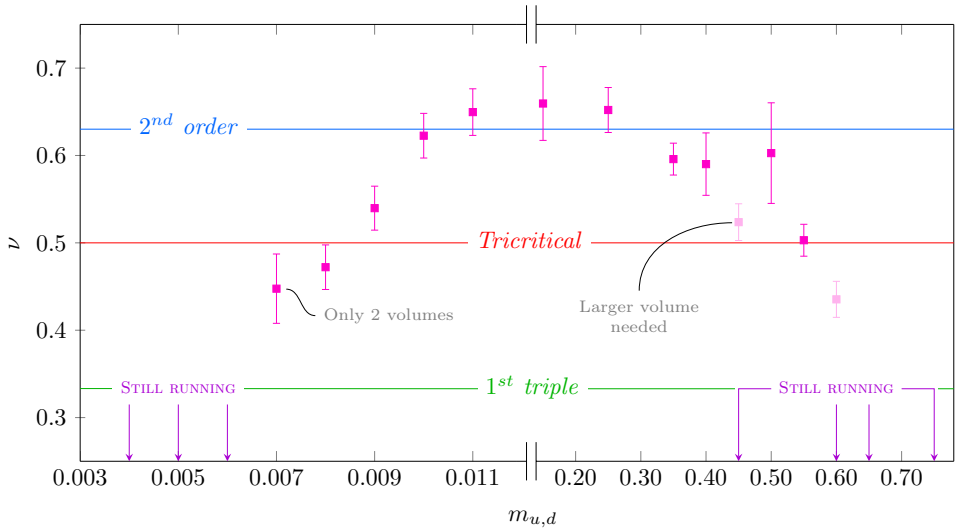

Figure 2.5: Critical exponent ν against bare mass $m_{u,d}$, taken from [14, p.5, figure 3]. The horizontal lines represent the critical values of ν for different universality classes.

In general, the boundaries of the different regions of fig. 2.4 will move approaching the continuum limit. Then, in particular at different N_τ, the pion mass m_π^{tric} will be different. Here we focus on the $N_\tau = 6$ result which has been presented in ref. [14]. Preliminary, it is claimed that in terms of bare lattice mass $a \cdot m_{u,d}$, the heavier tricritical point is at $m_{u,d}^{tric} = 0.55(10)a^{-1}$. Our aim is to understand which the corresponding pion mass is. The tricritical point can be determined by extraction of the critical exponent ν as it is done in ref. [15]. A plot for the critical exponent against the bare quark mass can

be found in figure 2.5. Having measured this pion mass and compared it to the experimental data for physical pions, one can qualitatively estimate the position of the physical point in the Columbia plot.

3 Lattice Spectroscopy

The aim of this thesis is to determine the pion mass in degenerate $N_f = 2$ lattice QCD for given bare up and down quark masses $m_{u,d}$. Thus we need to introduce a quantity which is directly connected to the particle mass. This quantity is the well-known correlator which depends on the properties of the observed particle. Since the pion is a meson, we only need a very simple form, namely the meson correlator.

3.1 Meson Correlators

The definition of the meson correlator $C(t)$ is given by (cf. [3, p.124])

$$C(n_t) = \langle M(n_t)\bar{M}(0)\rangle = \sum_k \langle 0|\,\hat{M}\,|k\rangle\,\langle k|\,\hat{M}^\dagger\,|0\rangle\, e^{-n_t\, a\, E_k} \tag{3.1}$$

$$= A\, e^{-n_t\, a\, E_M}(1 + \mathcal{O}(e^{-n_t\, a\, \Delta E})) \quad , \tag{3.2}$$

where E_M is the energy of the ground state, ΔE is the energy difference to the first excited state an $A \in \mathbb{R}$ is a constant. It is obvious that we can extract E_M of the meson from the leading exponential decay of the correlator.
With $M(n_t)$ we denote the meson interpolators, which are functionals of the lattice fields and defined by means of the corresponding Hilbert space operators creating and annihilating the particles to be analyzed

$$M(n) \equiv \bar{\psi}^{(f_1)}(n)\Gamma\psi(n)^{(f_2)} \tag{3.3}$$

$$\bar{M}(n) \equiv \bar{\psi}^{(f_2)}(n)\Gamma\psi(n)^{(f_1)} \quad . \tag{3.4}$$

Γ is a combination of Dirac matrices $\gamma_\mu, \mu = 1, \ldots, 4$ and γ_5 that provides the interpolator with the desired quantum numbers. f_1 and f_2 are again flavor indices. For example, using Wilson fermions the interpolator for the π^+ ($|\pi^+\rangle = \left|u\bar{d}\right\rangle$) reads [3, p.125]

$$M_{\pi^+}(n) = \bar{\psi}_d(n)\gamma_5\psi_u(n) = \bar{\psi}_d(n)_c^\alpha(\gamma_5)_{\alpha\beta}\psi_u(n)_c^\beta \quad . \tag{3.5}$$

In general, choosing $\Gamma = \gamma_5$ gives pseudoscalar mesons. Although in the staggered formulation there are 16 different pions because of the taste symmetry, we will only calculate the mass of the lightest one which is the pseudoscalar pion. In the continuum limit, all 16 pions become degenerate and therefore the continuum extrapolation for all pions would give the same result.

3.1.1 Zero Momentum Projection

Having a look at (3.2), one recognizes that the particle's mass does not enter the correlator directly but rather its energy. The energy E_M is directly related to the meson mass m_M through the relativistic dispersion relation, which on the lattice is given by [3, p.132]

$$E(\mathbf{p}) = \sqrt{m_M^2 + \mathbf{p}^2}\,(1 + \mathcal{O}(ap)) \tag{3.6}$$

$$\Rightarrow E(\mathbf{p} = \mathbf{0}) = E_0 = m_M \quad . \tag{3.7}$$

Hence, we have to perform the zero momentum projection which can be obtained by Fourier transformation of our meson interpolators into spatial momentum space [3, p.131]

$$\tilde{M}(\mathbf{p}, n_t) = \frac{1}{|\Lambda_3|} \sum_{\mathbf{n}\in\Lambda_3} M(\mathbf{n}, n_t)\, e^{-i\,a\,\mathbf{n}\mathbf{p}} \quad , \tag{3.8}$$

where $|\Lambda_3|$ expresses the spatial lattice volume and $\mathbf{p}$ the momentum.
Inserting (3.8) into (3.2) yields

$$C(t) = \langle \tilde{M}(\mathbf{p} = \mathbf{0}, n_t)\bar{M}(\mathbf{0}, 0)\rangle = A\, e^{-a\,n_t\,E_0}\,(1 + \mathcal{O}(e^{-a\,n_t\,\Delta E})) \quad . \tag{3.9}$$

With $C(t)$ in terms of (3.9) we found an expression allowing us to extract the meson mass directly.

3.1.2 Point Sources

We will see from sec. 3.3 that the main ingredient to get the correlator is the propagator D_f^{-1}, namely the inverse of the dirac operator. Taking this statement for granted for a moment let us discuss why it is in general not possible and neither necessary to calculate the full propagator. Each entry $D_f^{-1}(n|m)_{ba}$ provides the information for the propagation of a certain quark with flavor f from a given point (m, a) – usually called source – to an other point (n, b) – usually called sink –. The notation (m, a) implies a staggered field on site m with color a. Note that in the staggered formulation no Dirac index is present. Since we are using a lattice with extents $N_s = 16, N_t = 32$, the full propagator D_f^{-1} consists of $(16^3 \cdot 32 \cdot 3)^2 \sim \mathcal{O}(10^{11})$ complex entries and it is not sparse. Hence it is not possible to store it entirely during the simulation.
This suggests the idea of using point sources that reduce the information to only the propagation from one fixed point to any site of the lattice. Therefore we just multiply the full propagator with the point source $S_0^{m_0,a_0}$ (cf. [3, p.135])

$$S_0^{(m_0,a_0)}(m)_a = \delta(m - m_0)\delta_{a,a_0} \tag{3.10}$$

$$\Rightarrow \sum_{m,a} D^{-1}(n|m)_{ba}\, S_0^{(m_0,a_0)}(m)_a = D^{-1}(n|m_0)_{b,a_0} \quad . \tag{3.11}$$

$D^{-1}(n|m_0)_{b,a_0}$ is nothing but a single column of the full propagator and therefore has the structure of a usual Dirac field on the lattice[1]. The loss of information gets in some ways recovered since we will average over the correlator results for randomly chosen point sources during the simulation. Thus, with a total number chosen high enough, the statistical deviations due to the use of point sources should be negligible.

3.2 Effective Mass

Having a closer look on the euclidean meson correlator, it can be observed that it is influenced by many relevant contributions besides the lowest energy E_0 we are interested in. Since (3.9) also reads as ([3, p.144])

$$C(n_t) = A_0 e^{-n_t\, E_0} \underbrace{[\, + A_1 e^{-n_t\, E_1} + \ldots]}_{\text{neglected terms}} \quad , \tag{3.12}$$

this contribution varies with n_t. But for increasing n_t at some point the ground state E_0 becomes the dominating one, i.e. the $\log(C(n_t))$-n_t plot becomes linear. Therefore, the effective mass m_{eff} is defined via [3, p.145]

$$m_{\text{eff}}\left(n_t + \frac{1}{2}\right) = \ln\left(\frac{C(n_t)}{C(n_t+1)}\right) \quad . \tag{3.13}$$

Once n_t is high enough (in our case this will be at $n_t > 7$), m_{eff} becomes constant in n_t and shapes the so-called effective mass plateau.
Another import fact when talking about the correlator is its symmetry with respect to the $n_t = N_T/2$ -axis due to the periodic boundary conditions of the lattice (i.e. $n_t \pm N_T = n_t$). This explains the typical *cosh*-behavior of the correlator

$$A_0\, e^{-n_t E_0} + A_0\, e^{-(N_T - n_t)E_0} = 2A_0 e^{-N_t E_0/2} \cosh((N_T/2 - n_t)E_0) \quad . \tag{3.14}$$

Taking that into account, one sets

$$\frac{C(n_t)}{C(n_t+1)} = \frac{\cosh(m_{\text{eff}}(n_t - N_T/2))}{\cosh(m_{\text{eff}}(n_t + 1 - N_T/2))} \tag{3.15}$$

and solves (3.15) for m_{eff} at each n_t. A two parameter fit in the region of the effective mass plateau provides a very good approximation for the mass of the desired particle in lattice units.

[1] Observe that this aspect plays a major role for code implementation (see chapter 5)

3.3 The Staggered Pseudoscalar Pion Correlator

We now want to take a closer look to the calculation of the staggered pseudoscalar pion correlator. First of all, we need to find the expressions for the corresponding interpolators $M(n_t)$, $\bar{M}(n_t)$ used in (3.9). A complete, though not very explicit analysis is given in ref. [16] with useful references to ref. [17] and ref. [18]. Especially the connection between the staggered fields on the finer lattice and the physical fields on the coarser lattice turns out to be non-trivial.
As stated in ref. [16, pp.877-881], we find

$$M(n_t) = \sum_{\vec{A}} \Phi(\vec{A}) M_{\vec{A}\langle\vec{A}+\vec{\delta}\rangle} \tag{3.16}$$

$$M_{\vec{A}\vec{B}}(n_t) = \sum_{\vec{x}\in\mathbb{Z}^3} \delta_{ab} D_{\vec{A}}\, \bar{\chi}_a(2\vec{x}) D_{\vec{B}}\, \chi_b(2\vec{x}) \tag{3.17}$$

$$D_{\vec{A}}\, \chi(2\vec{x}) = \sum_{\delta_1=\pm1} \sum_{\delta_2=\pm1} \sum_{\delta_3=\pm1} \chi(2\vec{x} + \delta_1 A_1 \vec{e}_1 + \delta_2 A_2 \vec{e}_2 + \delta_3 A_3 \vec{e}_3) \quad , \tag{3.18}$$

where for the pseudoscalar pion $\Phi(\vec{A})$ and $\vec{\delta}$ are given by

$$\Phi(\vec{A}) = (-1)^{A_1+A_2+A_3}, \quad \vec{\delta} = \vec{0} \quad . \tag{3.19}$$

In (3.16), the summation in $\vec{A}$ is taken over a unit cube, i.e. $\vec{A} = (\frac{1}{2} \pm \frac{1}{2}, \frac{1}{2} \pm \frac{1}{2}, \frac{1}{2} \pm \frac{1}{2})$, and $\langle\vec{A} + \vec{\delta}\rangle$ resides within a unit cube. The $\chi(\vec{x})$ are the staggered fermionfields on the finer lattice and $\vec{e}_k,\ k = 1, 2, 3$ in (3.18) are the usual unit vectors in 3d euclidean spatial space. The sum with respect to $\vec{x}$ is done summing over the coarser lattice, but all the sites of the finer lattice are considered thanks to the drift operators $D_{\vec{A}}$.
The aim now is to obtain an expression of $\bar{M}(n_t)$ with the sum performed over the lattice sites of the finer lattice and not of the coarser. This is because in any implementation, everything is calculated using the finer lattice.
Inserting (3.19) into (3.16) yields to

$$M(n_t) \ = \ \sum_{\vec{A}} (-1)^{A_1+A_2+A_3} M_{\vec{A},\vec{A}} \tag{3.20}$$

$$\overset{3.17}{=} \sum_{\vec{A}} (-1)^{A_1+A_2+A_3} \sum_{\vec{x}\in\mathbb{Z}^3} D_{\vec{A}}\, \bar{\chi}(2\vec{x}) D_{\vec{A}}\, \chi(2\vec{x}) \quad , \tag{3.21}$$

where we dropped the color indices a, b in second line as they are connected via a delta function $\delta_{a,b}$ anyway. In (3.21) we have two drift operators in a row. If one writes out this expression explicitly, fields that are not living in the same unit cube will occur. Since the summation index $\vec{A}$ is the same, we can put it in front, i.e. $D_{\vec{A}}\, \bar{\chi}(2\vec{x}) D_{\vec{A}}\, \chi(2\vec{x}) \to D_{\vec{A}}[\bar{\chi}(2\vec{x})\chi(2\vec{x})]$. Golterman called this step the *reduction rule* (see. [17, p.334])[2]. Simply discarding the terms in

[2]The main argument provided in this paper is that the discarded terms do not change the transformation properties of the remaining operator.

(3.21) where the two χ do not fit into the same unit cube on the spatial lattice leads to the wrong result in the end.
Furthermore we introduce the notation $\bar{\chi}(\vec{z})\chi(\vec{z}) \equiv \bar{\chi}\chi(\vec{z})$, so that (3.21) can be written as

$$M(n_t) = \sum_{\vec{x}\in\mathbb{Z}^3} \sum_{\vec{A}} (-1)^{A_1+A_2+A_3} D_{\vec{A}}[\bar{\chi}\chi(2\vec{x})] \quad . \tag{3.22}$$

Writing the sum on $\vec{A}$ in (3.22) explicitly gives

$$\begin{aligned} M(n_t) = \sum_{\vec{x}\in\mathbb{Z}^3} \{ & + D_{(0,0,0)}[\bar{\chi}\chi(2\vec{x})] \\ & - D_{(1,0,0)}[\bar{\chi}\chi(2\vec{x})] - D_{(0,1,0)}[\bar{\chi}\chi(2\vec{x})] - D_{(0,0,1)}[\bar{\chi}\chi(2\vec{x})] \\ & + D_{(1,1,0)}[\bar{\chi}\chi(2\vec{x})] + D_{(1,0,1)}[\bar{\chi}\chi(2\vec{x})] + D_{(0,1,1)}[\bar{\chi}\chi(2\vec{x})] \\ & - D_{(1,1,1)}[\bar{\chi}\chi(2\vec{x})]\} \quad . \end{aligned} \tag{3.23}$$

Inserting into (3.23) the explicit form of the drift operators $D_{\vec{A}}[\,\cdot\,]$ as defined in (3.18) leads to

$$\begin{aligned} M(n_t) = \sum_{\vec{x}\in\mathbb{Z}^3} \Big\{ & + 8\cdot\bar{\chi}\chi(2\vec{x}) - \Big[\sum_{k=1}^{3} 4\cdot\Big(\bar{\chi}\chi(2\vec{x}+\vec{e}_k) + \bar{\chi}\chi(2\vec{x}-\vec{e}_k)\Big)\Big] \\ & + \Big[\sum_{\substack{k,l=1\\k<l}}^{3} 2\cdot\Big(\bar{\chi}\chi(2\vec{x}+\vec{e}_k+\vec{e}_l) + \bar{\chi}\chi(2\vec{x}+\vec{e}_k-\vec{e}_l) \\ & \qquad + \bar{\chi}\chi(2\vec{x}-\vec{e}_k+\vec{e}_l) + \bar{\chi}\chi(2\vec{x}-\vec{e}_k-\vec{e}_l)\Big)\Big] \\ & - \Big[\bar{\chi}\chi(2\vec{x}+\vec{e}_1+\vec{e}_2+\vec{e}_3) + \bar{\chi}\chi(2\vec{x}+\vec{e}_1+\vec{e}_2-\vec{e}_3) \\ & + \bar{\chi}\chi(2\vec{x}+\vec{e}_1-\vec{e}_2+\vec{e}_3) + \bar{\chi}\chi(2\vec{x}+\vec{e}_1-\vec{e}_2-\vec{e}_3) \\ & + \bar{\chi}\chi(2\vec{x}-\vec{e}_1+\vec{e}_2+\vec{e}_3) + \bar{\chi}\chi(2\vec{x}-\vec{e}_1+\vec{e}_2-\vec{e}_3) \\ & + \bar{\chi}\chi(2\vec{x}-\vec{e}_1-\vec{e}_2+\vec{e}_3) + \bar{\chi}\chi(2\vec{x}-\vec{e}_1-\vec{e}_2-\vec{e}_3)\Big]\Big\} \quad . \end{aligned} \tag{3.24}$$

Now follows a crucial step. Since we have the sum over all $\vec{x} \in \mathbb{Z}^3$ in front of the expression in (3.24) and $\vec{x}$ only appears with a factor of 2, we reach the position $(2x, 2y, 2z)$ of any unit cube of the lattice and with the additional unit vectors we reach every point in a certain unit cube. It should be clear that the quantity $\bar{\chi}\chi$ in (3.24) appears at each lattice point. Actually it appears more than once at a given position. In fact, terms placed on the same vertex of different unit cubes can be put together due to the sum over $\vec{x} \in \mathbb{Z}^3$.
For example, $\bar{\chi}\chi(2\vec{x}+\vec{e}_1)$ and $\bar{\chi}\chi(2\vec{x}-\vec{e}_1)$ both are placed at position $(1, 0, 0)$ of

their unit cube, but the second term lives in a unit cube shifted one position in negative x-direction. More explicitly, $2\vec{x}-\vec{e}_1 = 2\vec{x}-2\vec{e}_1+\vec{e}_1 = 2(\vec{x}-\vec{e}_1)+\vec{e}_1 = 2\vec{x}' + \vec{e}_1$.
Sticking to this rule, (3.24) simplifies to

$$\begin{aligned} M(n_t) = \sum_{\vec{x}\in\mathbb{Z}^3} \Big[&+ 8\cdot\bar{\chi}\chi(2\vec{x}) - 8\cdot\bar{\chi}\chi(2\vec{x}+\vec{e}_1) - 8\cdot\bar{\chi}\chi(2\vec{x}+\vec{e}_2) - 8\cdot\bar{\chi}\chi(2\vec{x}+\vec{e}_3) \\ &+ 8\cdot\bar{\chi}\chi(2\vec{x}+\vec{e}_1+\vec{e}_2) + 8\cdot\bar{\chi}\chi(2\vec{x}+\vec{e}_1+\vec{e}_3) + 8\cdot\bar{\chi}\chi(2\vec{x}+\vec{e}_2+\vec{e}_3) \\ &- 8\cdot\bar{\chi}\chi(2\vec{x}+\vec{e}_1+\vec{e}_2+\vec{e}_3)\Big] \\ = 8\cdot\sum_{\vec{y}\in\mathbb{Z}^3} &(-1)^{(y_1+y_2+y_3)}\,\bar{\chi}\chi(\vec{y}) \\ = 8\cdot\sum_{\vec{y}\in\mathbb{Z}^3} &(-1)^{(y_1+y_2+y_3)}\,\bar{\chi}_{f_1}(\vec{y})\chi_{f_2}(\vec{y}) \quad . \end{aligned} \tag{3.25}$$

In the second step we switched the summation index from coarse ($\vec{x}$) to finer ($\vec{y}$) lattice and in the last one we explicitly reintroduced the flavor index. From (3.25) it is straightforward to obtain

$$\bar{M}(n_t) = 8\cdot\sum_{\vec{y}\in\mathbb{Z}^3} (-1)^{(y_1+y_2+y_3)}\,\bar{\chi}_{f_2}(\vec{y})\chi_{f_1}(\vec{y}) \tag{3.26}$$

(3.25) and (3.26) represent the final expressions for the staggered pseudoscalar pion interpolators. Inserting (3.25) and (3.26) into (3.9), the expression for the correlator looks as follows

$$\begin{aligned} C(n_t) &= 64\cdot\langle\sum_{\vec{x}\in\mathbb{Z}^3}(-1)^{x_1+x_2+x_3}\cdot\bar{\chi}^a_{f_1}(\vec{x})\chi^a_{f_2}(\vec{x})\bar{\chi}^b_{f_2}(\vec{0})\chi^b_{f_1}(\vec{0})\rangle_{F,G} \\ &= \underbrace{-64\cdot\sum_{\vec{x}\in\mathbb{Z}^3}(-1)^{x_1+x_2+x_3}\langle\chi^a_{f_2}(\vec{x})\bar{\chi}^b_{f_2}(\vec{0})\chi^b_{f_1}(\vec{0})\bar{\chi}^a_{f_1}(\vec{x})\rangle_{F,G}}_{\equiv R} \quad . \end{aligned} \tag{3.27}$$

Note that we have written the color index explicitly since both interpolators should have a one. The relative minus sign arises between the two lines because we performed an odd number of interchanges of the Grassmann variables χ. The fermion and gauge expectation value calculation is formulated in path integral representation with use of S_f, S_g as defined in (2.5) and (2.3)

$$C(n_t) = R\cdot\frac{\int DU[D\bar{\chi}\,D\chi]_{f_1,f_2}\chi^a_{f_2}(\vec{x})\bar{\chi}^b_{f_2}(\vec{0})\chi^b_{f_1}(\vec{0})\bar{\chi}^a_{f_1}(\vec{x})\cdot e^{-S_g-S_f}}{\int DU[D\bar{\chi}\,D\chi]_{f_1,f_2}e^{-S_g-S_f}} \tag{3.28}$$

As a remark, the gauge part of the path integral will be evaluated with the hybrid Monte Carlo algorithm which we will discuss in the next chapter. Furthermore, the result of (3.28) is well known and gives us the fermion propagators

(cf. [19, p.151])

$$\begin{aligned} C(n_t) &= R \cdot (D_{f_2}^{-1})^{ab}(\vec{x}|0)\,(D_{f_1}^{-1})^{ba}(0|\vec{x}) \\ &= R \cdot \mathrm{tr}\Big(D_{f_2}^{-1}(\vec{x}|0) D_{f_1}^{-1}(0|\vec{x})\Big) \end{aligned} \tag{3.29}$$

The trace in (3.29) is of course intended to be taken in color space. In order to simplify (3.29), we make use of the staggered η_5 hermiticity

$$\eta_5 D \eta_5 = D^\dagger \rightarrow \eta_5 D^{-1} \eta_5 = (D^{-1})^\dagger \tag{3.30}$$

$$\eta_5 = \eta_5^\dagger, \quad (\eta_5)^2 = \mathbb{1}, \quad \eta_5(x|y) = (-1)^{x_1+x_2+x_3+n_t}\delta_{x,y} \quad . \tag{3.31}$$

Hence, using (3.31) and (3.30), equation (3.29) turns into

$$\begin{aligned} C(n_t) &= R \cdot \mathrm{tr}\Big(D_{f_2}^{-1}(\vec{x}|0) D_{f_1}^{-1}(0|\vec{x})\Big) \\ &= R \cdot \mathrm{tr}\Big(D_{f_2}^{-1}(\vec{x}|0) [\eta_5 (D_{f_1}^{-1})^\dagger \eta_5](0|\vec{x})\Big) \\ &= -64 \cdot \sum_{\vec{x},\vec{y},\vec{z}\in\mathbb{Z}^3} (-1)^{x_1+x_2+x_3} \cdot D_{f_2}^{-1}(\vec{x}|0)\eta_5(0|\vec{y})(D_{f_1}^{-1})^\dagger(\vec{y}|\vec{z})\eta_5(\vec{z}|\vec{x}) \\ &= -64 \cdot \sum_{\vec{x}\in\mathbb{Z}^3} (-1)^{n_t} \cdot D_{f_2}^{-1}(\vec{x}|0)(D_{f_1}^{-1}(0|\vec{x}))^\dagger \\ &= -64 \cdot (-1)^{n_t} \sum_{\vec{x}\in\mathbb{Z}^3} D_{f_2}^{-1}(\vec{x}|0)(D_{f_1}^{-1}(\vec{x}|0))^* \\ &= -64 \cdot (-1)^{n_t} \sum_{\vec{x}\in\mathbb{Z}^3} |D_f^{-1}(\vec{x}|0)|^2 \quad . \end{aligned} \tag{3.32}$$

(3.32) represents our final expression for the staggered pseudoscalar pion correlator. Due to (3.9), we are only interested in the exponential decay of the correlator. Therefore we can drop the prefactor $-64 \cdot (-1)^{n_t}$ for the sake of simplicity without changing the value of the effective mass.
Comparing our result with the well known pion correlator in the Wilson formulation [3, p.136], we recognize that there is only a slight difference

$$\begin{aligned} C^S(n_t) &= -64 \cdot (-1)^{n_t} \sum_{\vec{x}\in\mathbb{Z}^3} \sum_{c,d} |(D_f^{-1}(\vec{x}|0))_{cd}|^2 \\ C^W(n_t) &= \quad - \quad \sum_{\vec{x}\in\mathbb{Z}^3} \sum_{\alpha,\beta,c,d} |(D_f^{-1}(\vec{x}|0))_{cd}^{\alpha\beta}|^2 \quad . \end{aligned} \tag{3.33}$$

Up to the negligible prefactor and the summation over the Dirac indices, the formulations are equivalent. The sum over the color indices tells us that we have to evaluate $D^{-1}(n|m_0)_{b,a_0}$ in (3.11) for three different sources, one for each possible color.

4 Numerics

As already mentioned before, the calculation of the gauge part of the expectation value in (3.28) requires the use of the hybrid Monte Carlo algorithm.

4.1 Hybrid Monte Carlo Algorithm

The hybrid Monte Carlo algorithm (HMC) is a Markov chain Monte Carlo method used to produce a sequence of random samples for a probability distribution where the direct sampling is quite complicated. In our case this probability distribution is given by e^{-S_g}, the exponential of the gauge part of the action. The sequences of random samples are called gauge configurations and are necessary for the numerical evaluation of the integral with an integrand distributed according to e^{-S_g}.
This integral is the gauge part of the expectation value we need to calculate in order to obtain the correlator. The HMC reduces its auto correlation by using the ergodic principle of molecular dynamics in the microcanonical ensemble.
Consider a general gauge expectation value $\langle A \rangle$, just like the one we want to calculate in (3.28), we find (cf. [3, p.73])

$$\langle A \rangle = \frac{1}{Z} \int \mathcal{D}[U] e^{S_g[U]} \, A[U] \quad \text{with} \quad Z = \int \mathcal{D}[U] e^{S_g[U]} \quad . \tag{4.1}$$

This expectation value $\langle A \rangle$ can be estimated by a simple average over the measurements on those configurations U

$$\langle A \rangle \approx \frac{1}{N} \sum_{n=1}^{N} A[U_n] \left(1 + \mathcal{O}(1/\sqrt{N})\right) \quad , \tag{4.2}$$

where U_n are distributed according to $e^{S_g[U]}$. The HMC starts with enlarging the partition function with momenta π (cf. [20, p.31])

$$Z = \int \mathcal{D}[\pi] \mathcal{D}[U] e^{-H(\pi, U)} \tag{4.3}$$

with $\mathcal{D}[\pi] = \prod_x d\pi_x$. The π_x are the associated momenta to the configurations U_x for each site x. The function H is given by

$$H(\pi, U) = \frac{1}{2} \sum_x \pi^2 + S_g[U] \quad . \tag{4.4}$$

Obviously this enlargement does not influence the expectation value $\langle A \rangle$ which only depends on U. We can now interpret H as hamiltonian of a molecular dynamic system, where U plays the role of a generalized position and our gauge action $S_g[U]$ is the potential energy of the system. Thus, the update of the configurations can be obtained by the evolution of the molecular dynamics system, which obeys Hamilton's equations of motion

$$\frac{dU}{d\tau} = \frac{\partial H}{\partial \pi} , \quad \frac{d\pi}{d\tau} = -\frac{\partial H}{\partial U} \quad . \tag{4.5}$$

with an artificial *Monte Carlo time* τ. We know from classical mechanics that the total energy H and the phase space volume ρ is conserved, i.e. $\frac{dH}{d\tau} = 0 = \frac{d\rho}{d\tau}$. Therefore, solving (4.5) for some initial configuration $(U(\tau), \pi(\tau))$ leads to a new configuration $(U'(\tau + \Delta\tau), \pi'(\tau + \Delta\tau))$ which is nothing but a microcanonical update. Due to the ergodic hypothesis one will reach every region of phase space after a number of steps chosen high enough and no region is distinguished.
The strategy for a complete HMC step is now firstly to apply a usual heat bath algorithm in order to create random momenta π and secondly update the fields ϕ with the micro canonical dynamics evolution. This is possible because the momenta are Gaussian distributed according to $P(\pi_i) \propto e^{-\pi_i^2/2}$ and independent of the configurations U. The use of several algorithms is the reason for the HMC to be called *hybrid*.
For the calculation of the equations of motion we use a numercial method that inevitably produces errors which would cause an inaccurancy of the HMC. Thus, we initially regard the new configuration (U', π') as a proposal for the Metropolis acceptance step. For this purpose we compute the change of the Hamiltonian ΔH and accept the new configuration with a probability of $e^{-\Delta H}$, i.e.

$$P_{acc} = min\left(1, e^{H(U',\pi') - H(U,\pi)}\right) \quad . \tag{4.6}$$

Note that in case of an exact (analytically) computation of 4.5 the change of variables is always accepted, since $\frac{dH}{d\tau} = 0$.
A full HMC step is composed of the following three steps:

1. heat bath in order to obtain new random π
2. compute equations of motion in order to obtain (U', π')
3. acceptance - rejection step with P_{acc}

Performing this HMC step N times will give you $N_{\text{acc}} = \langle P_{\text{acc}} \rangle \cdot N$ different gauge configurations U. The ratio N_{acc}/N is called acceptance rate and can usually be adjusted from 60% to 80%. Note that there is a correlation between consecutive configurations since the acceptance of the new configuration depends on the value of the old one. This correlation is called autocorrelation and plays a major role for the statistical analysis of the results.

4.2 Strategy of Mass Calculation

For this thesis there was used a $16^3 \times 32$ - lattice. The computations have been performed on the `L-CSC`[1] using the LQCD software CL^{2}QCD.
With the HMC there were 4 chains of gauge configurations and within each 200 configurations produced. During the procedure of gauge configurations production, every 50th trajectory was stored only in order to reduce the autocorrelation between the single configurations in one chain. Once the inverter which we will discuss in sec. 5.4 and the gaugefields have been put into the same folder, there were 8 sources with randomly chosen origin per gauge field inverted which resulted in 6400 different correlator files. The next step is to shift all the correlators measured on the same configuration in such a way that the source is placed at $n_t = 0$ and simply average them. In this way we produce one file per configuration instead of eight. Afterwards the correlators need to be folded with respect to the n_t-symmetry discussed in (3.14). All these steps were done with simple `python` and `bash` scripts.
Apparently, the crucial step is to take the gauge average over all correlators in order to obtain one final correlator. This step is not straight forward because of the necessity to respect the autocorrelations of the data.
In this thesis the Γ-method is used in order to take the gauge average. The Γ-method is a general tool to treat Monte Carlo data which provides much better statistical analysis than standard procedures like binning etc. Without going into further detail, the Γ-method approximates the autocorrelation function in order to minimize statistical error. The `matlab` routine by Prof. Ulli Wolff was the method of choice for this thesis. Further information about the Γ-method and the `matlab` routine can be found in ref. [21].
The 4 so-called replica per 200 correlators each go into the `matlab` routine by Ulli Wolff which gives us as output one final correlator as well as the effective mass as function of n_t and the final pion mass fitted on the effective mass plateau. These results are presented in chapter 6.

[1] `https://www.top500.org/news/the-inside-story-of-lattice-csc-1\ -supercomputer-on-the-green500/`

5 Code - Implementation

5.1 CL^{2}QCD - an Overview

CL^{2}QCD stands for (Open)CL lattice QCD. It is a software for lattice QCD calculations using the programming language `OpenCL`[1]. `OpenCL` is among other things the most appropriate choice because it allows to perform calculations on graphic processing units (GPU). With the aid of multiple GPU it is possible to execute the calculations highly parallelized which accelerates their runtime. The `L-CSC` on which the measurements for this thesis have been done uses AMD FirePro^{TM} S9150 GPUs.
As a crude comparison, one could pretend a screen with its many pixels as a lattice with many lattice points. If a screen wants to display the next picture, all pixels are updated simultaneously and somehow this procedure can be transferred onto a lattice, where the values of the field on every lattice site can be updated simultaneously on every time slice in order to process much faster to the next slice.
CL^{2}QCD has been developed by the working group of Prof. Philipsen at the Goethe Universität Frankfurt (ref. [22]) and first was intended to be a hybrid Monte Carlo algorithm only. It is a public software and available as a git[2]. In the following it will be referred to the structure of the code as done in [22].
With increasing awareness of its utility the functionality of CL^{2}QCD was extended to several executables such as the producing of gauge configurations, the measurement on gauge configurations and the spectroscopy for Wilson fermions. The host program is written in `C++11` containing all the code that is responsible for file writing, parameter handling, etc. Whenever there occur bigger calculation steps, this main program calls kernels written in `OpenCL`. In this thesis the functionality of spectroscopy for staggered fermions was added, yet restricted to the pseudoscalar pion. For that purpose there were written two kernels, namely one for the point source implementation and the other one for the correlator calculation. The staggered correlator module can be found in `hardware::code`.

[1] `https://www.khronos.org/opencl/`
[2] `https://github.com/CL2QCD/cl2qcd`

5.2 Point Source and Correlator Implementation

A pseudocode for the implementation of the point sources is given in algorithm 1. The position of the point sources is randomly chosen. In principle

Algorithm 1 point source implementation

Require: a_0, m_0 ▷ color index a_0 and lattice site m_0
Ensure: $S_0^{(m_0,a_0)}(m)_a$ ▷ point source at (a_0, m_0) (cf. 3.11)

```
for n_t := 0 to N_t − 1 step 1 do
    for n_1, n_2, n_3 := 0 to N_s − 1 step 1 do   ▷ n = (n_1, n_2, n_3, n_t) (cf. 2.5)
        for b := 0 to 2 step 1 do
            if n = m and b = a then
                S_0^(m_0,a_0)(n)_b ← 1
            else
                S_0^(m_0,a_0)(n)_b ← 0
            end if
        end for
    end for
end for
return S_0^(m_0,a_0)(m)_a
```

this code does nothing more but assign the value `1` to only a single entry of the sourcefield and set all others to zero. This means that we access the array at the lattice point where our source shall be placed on and where one of the three color components is set to `1`. Note that for one lattice point we actually average over three sources that do only differ in their color.
The correlator is calculated with the help of a kernel which is sketched in algorithm 2. Since we neglect the prefactors for the correlator, the code becomes quite easy. Note that the total field consists of three component arrays for the three colors on every lattice point. Thus taking the Euclidean norm of a field at a certain position means nothing more but to compute the Euclidean norm of a complex three component vector in euclidean space.
The division of the correlator value by the spatial volume for every timeslice is just done for reasons of normalization. Since we have already discussed the negligibility of appearing prefactors, one could as well leave that step out.

5.3 Even - Odd Preconditioning

In favor of reducing the run-time of the code we introduced the even - odd preconditioning. In favor the lattice is separated into two different ones, namely

Algorithm 2 correlator calculation

Require: $D^{-1}(n|m_0)_{a_0}$ ▷ propagator/inv. source for fixed lattice site m_0 and color a_0

Ensure: $C(n_t),\ n_t \in \mathbb{N}^0,\ 0 \leq n_t \leq N_t$ ▷ updated correlator for one inverted source

1: **for** $n_t := 0$ **to** $N_t - 1$ **step** 1 **do**
2: $\quad \mathrm{tmp}(n_t) \leftarrow 0$ ▷ temporal correlator
3: $\quad$ **for** $n_1, n_2, n_3 := 0$ **to** $N_s - 1$ **step** 1 **do** ▷ $n = (n_1, n_2, n_3, n_t)$ (cf. 2.5)
4: $\quad\quad \mathrm{tmp}(n_t) \leftarrow \mathrm{tmp}(n_t) + |D^{-1}(n|m_0)_{a_0}|^2$ ▷ usual squarenorm for 3 component vector
5: $\quad$ **end for**
6: $\quad C(n_t) \leftarrow \mathrm{tmp}(n_t)/N_s^3$ ▷ normalization with spatial volume
7: **end for**
8: **return** $C(n_t)$

the even and the odd part. For $n \in \Lambda$ we define

$$n \text{ is called } \begin{cases} \text{even, if :} & (n_1+n_2+n_3+n_t)/2 \in \mathbb{N} \\ \text{odd, if :} & (n_1+n_2+n_3+n_t)/2 \notin \mathbb{N} \end{cases} . \tag{5.1}$$

Taking this into account, we can split up fields φ and matrices A on the lattice into an even an an odd part

$$A := \begin{pmatrix} A_{ee} & A_{eo} \\ A_{oe} & A_{oo} \end{pmatrix},\ \varphi := \begin{pmatrix} \varphi_e \\ \varphi_o \end{pmatrix},\ A \cdot \varphi = \begin{pmatrix} A_{ee}\varphi_e & A_{eo}\varphi_o \\ A_{oe}\varphi_e & A_{oo}\varphi_o \end{pmatrix} , \tag{5.2}$$

where obviously index e stands for even and o for odd. Furthermore we can rewrite our staggered fermionic action (2.21) in terms of

$$S_F^{(stag.)} = \bar{\chi}(\not{D} + \hat{M}_0)\chi = \bar{\chi} D \chi \text{ with } D = \begin{pmatrix} \hat{M}_0 \mathbb{1} & D_{eo} \\ D_{oe} & \hat{M}_0 \mathbb{1} \end{pmatrix} . \tag{5.3}$$

Having D defined just like in (5.3), we find the properties

$$D^\dagger = \begin{pmatrix} \hat{M}_0 \mathbb{1} & D_{oe}^\dagger \\ D_{eo}^\dagger & \hat{M}_0 \mathbb{1} \end{pmatrix} = D^{-1}, \text{ since } D_{eo}^\dagger = -D_{oe}\ ,\ D_{oe}^\dagger = -D_{eo}\ ; \tag{5.4}$$

$$D^\dagger D = \begin{pmatrix} \hat{M}_0^2 \mathbb{1} - D_{eo}D_{oe} & \mathbb{O} \\ \mathbb{O} & \hat{M}_0^2 \mathbb{1} - D_{oe}D_{eo} \end{pmatrix} = \begin{pmatrix} (D^\dagger D)_{ee} & \mathbb{O} \\ \mathbb{O} & (D^\dagger D)_{00} \end{pmatrix} . \tag{5.5}$$

The aim of even - odd preconditioning is to facilitate the computational extremely expensive step of inversion as done in (3.11). Let S^0 be our source, than we can write (3.11) as

$$D^{-1}S^0 = D^\dagger (D^\dagger D)^{-1} S^0 = D^\dagger \begin{pmatrix} (D^\dagger D)_{ee}^{-1} & \mathbb{O} \\ \mathbb{O} & (D^\dagger D)_{oo}^{-1} \end{pmatrix} \begin{pmatrix} S_e^0 \\ S_o^0 \end{pmatrix} := \begin{pmatrix} \chi_e \\ \chi_o \end{pmatrix} . \tag{5.6}$$

With χ we denote our inverted source or propagator. Because our source S^0 is either placed on an even or on an odd site,only one of the two components S^0_e and S^0_o is unequal to zero.
Let us first suppose $S^0_o = 0$, then (5.6) reads

$$\begin{aligned}\begin{pmatrix} \chi_e \\ \chi_o \end{pmatrix} &= \begin{pmatrix} \hat{M}_0 \mathbb{1} & -D_{eo} \\ -D_{oe} & \hat{M}_0 \mathbb{1} \end{pmatrix} \begin{pmatrix} (D^\dagger D)^{-1}_{ee} S^0_e \\ 0 \end{pmatrix} \\ &= \begin{pmatrix} \hat{M}_0 \cdot (D^\dagger D)^{-1}_{ee} S^0_e \\ -D_{oe} \cdot (D^\dagger D)^{-1}_{ee} S^0_e \end{pmatrix} = \begin{pmatrix} \hat{M}_0 \phi_e \\ -D_{oe} \phi_e \end{pmatrix} \quad , \end{aligned} \tag{5.7}$$

where we have introduced $\phi_e := (D^\dagger D)^{-1}_{ee} S^0_e$ as an auxiliary variable.
One can perform the same calculation for a source on an odd site, i.e. $S^0_e = 0$, and one will end up with

$$\begin{pmatrix} \chi_e \\ \chi_o \end{pmatrix} = \begin{pmatrix} -D_{eo} \phi_o \\ \hat{M}_0 \phi_o \end{pmatrix} , \quad \phi_o := (D^\dagger D)^{-1}_{oo} S^0_o \quad . \tag{5.8}$$

The only inversion left we have to calculate is the one on the ϕ_e respectively ϕ_o. This inversion is much cheaper as it is only performed on half the lattice to the price of having to check every source for being even or odd.

5.4 Inverter Executable

The function `measurePseudoscalarCorrelatorOnGaugefieldAndWriteToFile` in `physics::observables::staggered` brings together the source creation, the source inversion and the correlator calculation and writes the results into an output-file. Algorithm 3 gives an overview of this main function. Note that the gaugefield is needed in order to perform the inversion. This function is called if the inverter executable is run. Different options can be given to this executable, a possible example is

```
./inverter
--sourcefile=conf.05100 --use_cpu=false --fermact=rooted_stagg
--ferm_obs_corr_postfix=_5_5_7_20_corr --log-level=info
--source_x=5 --source_y=5 --source_z=7 --source_t=20 --corr_dir=0
--beta=5.8108 --mass=0.5500 --cgmax=30000 --use_chem_pot_im=0
--cg_iteration_block_size=50 --startcondition=continue
--theta_fermion_temporal=1 --num_sources=3 --ns=16 --nt=32
```

Algorithm 3 main function

Require: gaugefield, m_0 ▷ m_0 position of pointsource
Ensure: output-file with correlator
1: $C(n_t) \leftarrow 0 \forall n_t$
2: **for** $a_0 := 0$ **to** 2 **step** 1 **do**
3: **call** algorithm 1
4: **if** source on even site **then**
5: perform inversion according to 5.7
6: **else**
7: perform inversion according to 5.8
8: **end if**
9: $\rightarrow D^{-1}(n|m_0)_{a_0}$ **obtained** ▷ $D^{-1}(n|m_0)_{a_0}$ propagator/inv. source with color a_0
10: **call** algorithm 2 $\rightarrow C(n_t)$ **updated**
11: **end for**
12: $\rightarrow C(n_t)$ **obtained**
13: **write** $C(n_t)$ **to file**

6 Simulation Results

6.1 Pseudoscalar Pion Mass

The results of the final correlator can be found in tabular 6.1.

n_t	$C(n_t)$	$\Delta C(n_t)$	$\Delta(\Delta C(n_t))$
0	3.733090×10^{-4}	1.945233×10^{-7}	8.423105×10^{-9}
1	6.253498×10^{-5}	4.419093×10^{-8}	1.913523×10^{-9}
2	1.079353×10^{-5}	8.767617×10^{-9}	3.796489×10^{-10}
3	1.889187×10^{-6}	1.593477×10^{-9}	6.899960×10^{-11}
4	3.330698×10^{-7}	3.046142×10^{-10}	1.319018×10^{-11}
5	5.898075×10^{-8}	5.571973×10^{-11}	2.412735×10^{-12}
6	1.047056×10^{-8}	1.002845×10^{-11}	4.342444×10^{-13}
7	1.860808×10^{-9}	1.859911×10^{-12}	8.053652×10^{-14}
8	3.310442×10^{-10}	3.427287×10^{-13}	1.484059×10^{-14}
9	5.891956×10^{-11}	6.241772×10^{-14}	2.702767×10^{-15}
10	1.048579×10^{-11}	1.130043×10^{-14}	4.893228×10^{-16}
11	1.866326×10^{-12}	2.043117×10^{-15}	8.846957×10^{-17}
12	3.321680×10^{-13}	3.677161×10^{-16}	1.592257×10^{-17}
13	5.911842×10^{-14}	6.573397×10^{-17}	2.846364×10^{-18}
14	1.053688×10^{-14}	1.177513×10^{-17}	5.098781×10^{-19}
15	1.932870×10^{-15}	2.215307×10^{-18}	9.592562×10^{-20}
16	6.670215×10^{-16}	7.815868×10^{-19}	4.369203×10^{-20}

Table 6.1: Staggered pseudoscalar pion correlator data calculated with CL^{2}QCD

Applying the Γ-method gives us the effective mass (see tab. 6.2).
The plot for the effective mass can be found in figure 6.1.
The green line in fig. 6.1 represents the two-parameter-fit in the region of the effective mass plateau. The value given in the figure is the one that is obtained by applying the standard χ^2 method in `gnuplot`.
The Γ-method claims a more precise but slightly different result of

$$a \cdot m_{\text{eff}} = 1.7259(3) \quad . \tag{6.1}$$

n_t	$a \cdot m_{eff}(n_t)$	$\Delta a \cdot m_{eff}(n_t)$	$\Delta(\Delta a \cdot m_{eff}(n_t))$
0	1.786680	4.125825×10^{-4}	1.786535×10^{-5}
1	1.756779	3.357311×10^{-4}	1.453758×10^{-5}
2	1.742800	3.052222×10^{-4}	1.321651×10^{-5}
3	1.735550	2.874748×10^{-4}	1.901467×10^{-5}
4	1.731141	2.468868×10^{-4}	1.380139×10^{-5}
5	1.728643	2.318702×10^{-4}	1.296194×10^{-5}
6	1.727557	2.132432×10^{-4}	9.233702×10^{-6}
7	1.726514	1.880430×10^{-4}	8.142502×10^{-6}
8	1.726079	1.752592×10^{-4}	7.588944×10^{-6}
9	1.726152	1.765309×10^{-4}	9.868375×10^{-6}
10	1.726049	1.596598×10^{-4}	6.913472×10^{-6}
11	1.726087	1.528588×10^{-4}	6.618979×10^{-6}
12	1.726129	1.403803×10^{-4}	6.078643×10^{-6}
13	1.725634	1.331916×10^{-4}	5.767365×10^{-6}
14	1.726059	1.407297×10^{-4}	6.093774×10^{-6}
15	1.725888	3.013024×10^{-4}	1.304678×10^{-5}

Table 6.2: Effective mass for pseudoscalar pion calculated by apllying the Γ-method to the data of tab. 6.1

The advisor of the thesis, Ph.D. Alessandro Sciarra, has recently calculated the lattice spacing a in context of his proceeding Ph.D. thesis and provided the result for our purpose.

$$a = 0.1212(13) \text{ fm} \tag{6.2}$$

The calculation was done for staggered fermions in the same way as it was done in [15] for Wilson fermions.
Thus we can specify the pseudoscalar pion mass in physical units

$$m_\pi = m_{\text{eff}} \cdot a^{-1} \cdot (\hbar c) = 2.81(3) \text{ GeV} \quad . \tag{6.3}$$

6.2 Discussion

Compared to the real physical pion mass of 134.9766(6) MeV our mass of $m_\pi = 2.81(3)$ GeV is about a factor of 20 higher. This was expectable since we used quark masses quite heavier than in nature.
One notes that the pion mass in lattice units which is given by $m_{\text{eff}} = 1.7259(3) \cdot a^{-1}$ is higher than one. This means that the pion is not resolved completely within our lattice since its Compton wavelength is bigger than a. Nevertheless in lattice literature it is common to use values for particle masses in lattice units below two. There are methods to make sense of numbers like this which

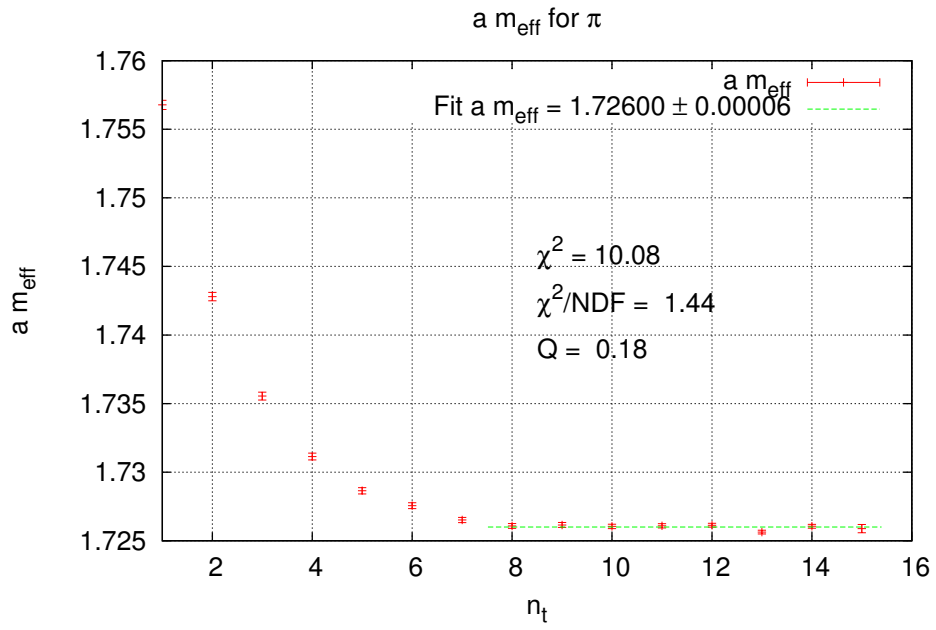

Figure 6.1: Effective mass against n_t plot for pseudoscalar pion with effective mass plateau fit done with `gnuplot`

we do not want to discuss in this thesis.
In order to minimize the pion mass in lattice units, one needs a lattice with bigger N_τ which implies smaller lattice spacing a that may be appropriate for the pion Compton wavelength.

The result itself tells us something about the position of the heavier tricritical point on the $N_f = 2$ line in the Roberge-Weiss plane. Even though the deconfinement first order region enlarges in the continuum limit, we are with a factor of 20 so far removed from the physical mass, that probably the projection of the physical point on the Roberge-Weiss plane is placed in the Z_2 region. This assumption is coherent with the current status of research (see ref. [23]).

Summary and Outlook

In this thesis we implemented the procedure for staggered pseudoscalar pion mass spectroscopy in the LQCD software CL^{2}QCD. For this reason we studied the staggered formalism for spectroscopy on the lattice. This approach was time consuming because it is not as straight forward as in the Wilson case. This software is a completely general tool which enables the application of the spectroscopy procedure for any given bare quark mass. We used the technique of point sources only because it is sufficient for the purpose of pion spectroscopy.
We measured the corresponding pion mass given the tricritical heavier bare quark mass in the Roberge-Weiss plane for $N_f = 2$. We then put into physical context.

The determination of the lighter tricitical point as well as the physical point(i.e. the measured pion mass is equal to the physical pion mass) are reasonable applications in future in order to give more detailed statements on the structure of the Columbia plot.

Bibliography

[1] Wikipedia, "Standard model — wikipedia, the free encyclopedia," 2016. https://en.wikipedia.org/w/index.php?title=Standard_Model&oldid=748503028. [Online; accessed 8-November-2016].

[2] **Particle Data Group** Collaboration, C. Patrignani *et al.*, "Review of Particle Physics," *Chin. Phys.* **C40** no. 10, (2016) 100001.

[3] C. Gattringer and C. Lang, *Quantum Chromodynamics on the Lattice - An Introductory Presentation*. Springer Science & Business Media, Berlin Heidelberg, 2009.

[4] H. J. Rothe, *Lattice Gauge Theories - An Introduction*. World Scientific, Singapur, third. ed., 2005.

[5] T. DeGrand and C. DeTar, *Lattice Methods for Quantum Chromodynamics*. World Scientific, Singapore, 2006. https://cds.cern.ch/record/1055545.

[6] S. Sharpe, "Rooted staggered fermions: good, bad or ugly?," in *XXIVth International Symposium on Lattice Field Theory*, p. 22.1. Dec., 2006. hep-lat/0610094.

[7] H. Satz, "The Quark-Gluon Plasma - A Short Introduction," *Nuclear Physics A* **862** (July, 2011) 4–12, arXiv:1101.3937 [hep-ph].

[8] D. H. Rischke, "The quark-gluon plasma in equilibrium," *Progress in Particle and Nuclear Physics* **52** (Mar., 2004) 197–296, nucl-th/0305030.

[9] P. Petreczky, "Lattice QCD at non-zero temperature," *Journal of Physics G Nuclear Physics* **39** no. 9, (Sept., 2012) 093002, arXiv:1203.5320 [hep-lat].

[10] K. Fukushima and T. Hatsuda, "The phase diagram of dense QCD," *Reports on Progress in Physics* **74** no. 1, (Jan., 2011) 014001, arXiv:1005.4814 [hep-ph].

[11] O. Philipsen and C. Pinke, "$N_f = 2$ qcd chiral phase transition with wilson fermions at zero and imaginary chemical potential," *Phys. Rev. D*

93 (Jun, 2016) 114507.
http://link.aps.org/doi/10.1103/PhysRevD.93.114507.

[12] A. Roberge and N. Weiss, "Gauge Theories With Imaginary Chemical Potential and the Phases of QCD," *Nucl. Phys.* **B275** (1986) 734–745.

[13] C. Bonati, P. de Forcrand, M. D'Elia, O. Philipsen, and F. Sanfilippo, "Chiral phase transition in two-flavor qcd from an imaginary chemical potential," *Phys. Rev. D* **90** (Oct, 2014) 074030.
http://link.aps.org/doi/10.1103/PhysRevD.90.074030.

[14] O. Philipsen and A. Sciarra, "Roberge-Weiss transition in $N\_f = 2$ QCD with staggered fermions and $N\_\tau = 6$," *ArXiv e-prints* (Oct., 2016) , arXiv:1610.09979 [hep-lat].

[15] C. Czaban, F. Cuteri, O. Philipsen, C. Pinke, and A. Sciarra, "Roberge-weiss transition in $\mathrm{n_f} = 2$ qcd with wilson fermions and $\mathrm{n}_\tau = 6$," *Phys. Rev. D* **93** (Mar, 2016) 054507.
http://link.aps.org/doi/10.1103/PhysRevD.93.054507.

[16] N. Ishizuka, M. Fukugita, H. Mino, M. Okawa, and A. Ukawa, "Operator dependence of hadron masses for Kogut-Susskind quarks on the lattice," *Nucl. Phys.* **B411** (1994) 875–902.

[17] M. F. Golterman and J. Smit, "Lattice baryons with staggered fermions," *Nuclear Physics B* **255** (Jan, 1985) 328–340.
http://dx.doi.org/10.1016/0550-3213(85)90138-5.

[18] M. F. Golterman, "Staggered mesons," *Nuclear Physics B* **273** no. 3-4, (Sep, 1986) 663–676.
http://dx.doi.org/10.1016/0550-3213(86)90383-4.

[19] M. D. Schwartz, *Quantum Field Theory and the Standard Model* -. Cambridge University Press, Cambridge, new. ed., 2014.

[20] C. Pinke, *Lattice QCD at Finite Temperature with Wilson Fermions*. PhD thesis, 2014. http://publikationen.ub.uni-frankfurt.de/frontdoor/index/index/docId/35074.

[21] U. Wolff and Alpha Collaboration, "Monte Carlo errors with less errors," *Computer Physics Communications* **156** (Jan, 2004) 143–153, hep-lat/0306017.

[22] O. Philipsen, C. Pinke, A. Sciarra, and M. Bach, "CL2QCD - Lattice QCD based on OpenCL," *ArXiv e-prints* (Nov., 2014) , arXiv:1411.5219 [hep-lat].

[23] C. Bonati, M. D'Elia, M. Mariti, M. Mesiti, F. Negro, and F. Sanfilippo, "Roberge-Weiss endpoint at the physical point of $N_f = 2 + 1$ QCD," *Phys. Rev.* **D93** no. 7, (2016) 074504, `arXiv:1602.01426 [hep-lat]`.